2014

Transformation toughening in an antiferroelectric ceramic

Xiaoli Tan
Iowa State University, xtan@iastate.edu

S. E. Young
Iowa State University

Y.H. Seo
Technische Universitat Darmstadt

J.Y. Zhang
Iowa State University

W. Hong
Iowa State University

See next page for additional authors

Transformation toughening in an antiferroelectric ceramic

Abstract
Due to a larger specific volume of the ferroelectric phase, the antiferroelectric-ferroelectric transition is believed to have an enhanced toughening effect against fracture. The toughening requires a non-recoverable transformation in the crack process zone. Complementary measurement of the crystal symmetry, dielectric constant, field-induced polarization, and Raman spectrum on ceramic $Pb_{0.99}Nb_{0.02}[(Zr_{0.57}Sn_{0.43})_{0.92}Ti_{0.08}]_{0.98}O_3$ indicates that the antiferroelectric and the ferroelectric states are equally stable at room temperature. Raman mapping further reveals the presence of the ferroelectric phase in a localized zone at the crack tip after unloading. A significant phase-transition-toughening effect is demonstrated in the antiferroelectric ceramic with both indentation fracture and R-curve experiments. The effect in this model composition leads to toughness values ~50% larger than other antiferroelectric ceramics with similar compositions and 60 ~ 130% higher than ferroelectric $Pb(Zr,Ti)O_3$ ceramics. A simple analysis confirms the toughening effect from both volumetric phase transition and deviatoric domain switching during the transformation. The results suggest that other materials near phase boundaries may have similar high fracture resistance.

Keywords
Antiferroelectric ceramics; Phase transition toughening; Raman mapping; R-curve

Disciplines
Ceramic Materials | Electro-Mechanical Systems

Authors
Xiaoli Tan, S. E. Young, Y.H. Seo, J.Y. Zhang, W. Hong, and K. G. Webber

Acta Materialia 62, 114-121 (2014). DOI: 10.1016/j.actamat.2013.09.038.

Transformation toughening in an antiferroelectric ceramic

X. Tan[a,*], S.E. Young[a], Y.H. Seo[b], J.Y. Zhang[a], W. Hong[a], K.G. Webber[b]

[a]*Department of Materials Science and Engineering, Iowa State University, Ames, IA 50011, USA*

[b]*Institute of Materials Science, Technische Universität Darmstadt, 64287 Darmstadt, Germany*

Abstract Due to a larger specific volume of the ferroelectric phase, the antiferroelectric-ferroelectric transition is believed to have an enhanced toughening effect against fracture. The toughening requires a non-recoverable transformation in the crack process zone. Complementary measurement of the crystal symmetry, dielectric constant, field-induced polarization, and Raman spectrum on ceramic $Pb_{0.99}Nb_{0.02}[(Zr_{0.57}Sn_{0.43})_{0.92}Ti_{0.08}]_{0.98}O_3$ indicates that the antiferroelectric and the ferroelectric states are equally stable at room temperature. Raman mapping further reveals the presence of the ferroelectric phase in a localized zone at the crack tip after unloading. A significant phase-transition-toughening effect is demonstrated in the antiferroelectric ceramic with both indentation fracture and R-curve experiments. The effect in this model composition leads to toughness values ~50% larger than other antiferroelectric ceramics with similar compositions and 60 ~ 130% higher than ferroelectric $Pb(Zr,Ti)O_3$ ceramics. A simple analysis confirms the toughening effect from both volumetric phase transition and deviatoric domain switching during the transformation. The results suggest that other materials near phase boundaries may have similar high fracture resistance.

Keywords: Antiferroelectric ceramics; Phase transition toughening; Raman mapping; R-curve

*Corresponding author. Tel.: +1 515 294 3355; fax: +1 515 294 5444. E-mail address: xtan@iastate.edu (X. Tan)

1. Introduction

Ceramics are intrinsically prone to fracture [1], and toughening is always desired for structural as well as functional applications [2-5]. Among the various toughening mechanisms reported in monolithic ceramics, phase-transition toughening demonstrated in ZrO_2-based ceramics is probably the most effective one [4]. Other extrinsic toughening mechanisms in polycrystalline ceramics, such as ferroelastic toughening [6] or frictional crack bridging [7], are difficult to control without altering the electrical, mechanical, or electromechanical properties.

Antiferroelectric ceramics are promising candidates for dielectrics in high energy density electrical capacitors due to the electric field-induced antiferroelectric to ferroelectric phase transition [8-11]. This first order transition is manifested by the abrupt development of large electrical polarization and dimension expansion in both longitudinal and transverse directions in $PbZrO_3$-based perovskite compositions [12-18]. The associated volume change makes the phase transition sensitive to mechanical stress and hydrostatic pressure [11,12,15,19] and also raises reliability issues of actuators and capacitors utilizing antiferroelectric ceramics [20]. On the other hand, following the same working mechanism in ZrO_2-based structural ceramics, the volumetric strain at the phase transition in antiferroelectric materials may be exploited to toughen these functional electroceramics [21,22]. The most studied and documented toughening mechanism in functional electroceramics so far is ferroelastic toughening through localized domain switching [6,23-29]. Since $PbZrO_3$-based ceramics contain non-180^o antiferroelectric domains [30,31] and are ferroelastic prior to and after the phase transition [22,32], the ferroelastic toughening mechanism is still expected to contribute. In order for the volumetric phase-transition toughening to work in antiferroelectric ceramics, the induced ferroelectric phase must be stable at the crack tip after unloading [3]. Therefore, the composition of the ceramic needs to be fine-tuned to

achieve an irreversible antiferroelectric-to-ferroelectric phase transition at room temperature. In such an antiferroelectric composition, the combined effect of both ferroelastic-toughening and phase-transition-toughening mechanisms is expected, and as a result, an enhanced toughness will be observed.

2. Experimental

Our previous studies indicate that the compositions $y = 0.07 \sim 0.08$ in the solid solution $Pb_{0.99}Nb_{0.02}[(Zr_{0.57}Sn_{0.43})_{1-y}Ti_y]_{0.98}O_3$ (PNZST 43/100y/2) display an irreversible antiferroelectric to ferroelectric phase transition at room temperature [17,33]. Therefore, PNZST 43/8.0/2 is selected to demonstrate the phase-transition toughening effect. To produce the ceramic, powders of PbO, ZrO_2, SnO_2, TiO_2, and Nb_2O_5 with purity levels >99.9% were batched with an additional 5 wt.% PbO to compensate for PbO evaporation during calcination and sintering. Calcination was repeated twice at 935 °C for 4 hours for compositional homogeneity. Prior to each calcination, powder was vibratory milled for 7 hours in ethanol with zirconia media, dried, and pressed. After a final milling of 15 hours, 40 g of dried PNZST 43/8.0/2 powder was uniaxially pressed at ~75 MPa in a 43 mm diameter cylindrical die with acrylic binder. Cold isostatic pressing was then applied to the green compact at ~400 MPa. After the binder was burnt out at 450 °C, sintering was carried out at 1325 °C for 3 hours. A double crucible method was used for sintering with plenty of protective powder. To further increase the density of the ceramic, hot isostatic pressing were carried out at 1150 °C and ~200 MPa for 2 hours in a 20% O_2, 80% Ar atmosphere.

The density of the ceramic was measured with the Archimedes method, and the phase purity was analyzed with X-ray diffraction. Scanning electron microscopy was used to examine

the fracture surface of the ceramic, and the linear intercept method was used to determine average grain size.

The dielectric constant and dielectric loss tangent of PNZST 43/8.0/2 were measured at 1 kHz, 10 kHz, and 100 kHz with an LCZ meter (Model 3322, Keithley) during heating and cooling at a rate of 3 °C/min. The polarization vs. electric field hysteresis loop of the sample was recorded with a standardized ferroelectric test system (RT66A, Radiant Technologies) during the very first triangular wave cycle of a field at 4 Hz.

To reveal the ferroelectric phase induced by cooling, X-ray diffraction on the pseudocubic (200) peak with extended data collection time was conducted. The specimen was stored in a cooler with frozen carbon dioxide (-78 °C) for several hours just before the room temperature X-ray scan. To reveal the ferroelectric phase induced by the electric field, silver thin film electrodes were sputtered onto the specimen, and a DC field of 40 kV/cm was applied for 10 minutes. Then the silver films were dissolved with nitric acid, and the (200) peak was scanned on the broad face perpendicular to the poling direction.

For indentation fracture toughness assessment, Vickers indents were made by applying 0.5 kg of force for 13 seconds on the polished surface. The fracture toughness was estimated according to equations found in literature [34].

Fracture resistance (R) curves were measured on a compact-tension (CT) specimen with dimensions of 24 mm × 25 mm × 3 mm. Experimental details can be found in our previous report [29]. For the purpose of comparison, R-curve tests were also carried out on an antiferroelectric ceramic PNZST 43/6.4/2, which is very similar chemically to PNZST 43/8.0/2 but with a reversible antiferroelectric to ferroelectric phase transition.

Raman spectroscopy experiments were performed with a Renishaw inVia Raman spectrometer using a 488 nm wavelength laser at 20 mW. A 20× objective lens was used to collect a single spectrum on as-processed, cooled, and poled PNZST 43/8.0/2 specimens.

In addition, numerous spectra were collected to map the phase transition zone. For this purpose, a specimen with dimensions of 2 mm × 4 mm × 0.5 mm was polished and electroded. A Knoop indent was placed with 0.5 kgf for 13 seconds in the center of the polished surface with the longer diagonal perpendicular to the electric field direction. A 50× objective lens was used, which resulted in a laser spot size of ~3 μm. Raman mapping [35] was achieved by collecting spectra in the area around the indentation crack tip with step sizes of 2.5 μm (at virgin crack tip) and 3.0 μm (under electric field). A program in MATLAB® was created to compare the spectra and generate a contour map.

3. Results

Density measurements on PNZST 43/8.0/2 reveal that the ceramic prepared with hot isostatic pressing is 99% of theoretical density. X-ray diffraction indicates that the ceramic is phase pure with a pseudo-tetragonal perovskite structure (Fig. 1). The lattice parameters are determined to be $a = b = 4.105 \pm 0.001$ Å and $c = 4.081 \pm 0.001$ Å, which are consistent with our previous reports [11,17,33]. Scanning electron microscopy examination of the fracture surface (Fig. 2) confirms the high density and reveals an average grain size of 2.6 ± 0.3 μm.

Complimentary experiments were carried out on PNZST 43/8.0/2 to verify that both antiferroelectric and ferroelectric phases can be stabilized at room temperature in this composition. The results of the dielectric measurements are displayed in Fig. 3. During heating, a ferroelectric to antiferroelectric transition occurs at 43 °C, determined by the steepest point in the

loss tangent drop. On cooling, the antiferroelectric to ferroelectric transition occurs with a more gradual increase in loss tangent, centered at -8 °C. Additionally, the anomalies on dielectric constant curves correspond well to those of the loss tangent curves. The results hence indicate that the ceramic can be thermally manipulated to exist either in an antiferroelectric or in a ferroelectric state at room temperature (25 °C). The dielectric constant anomalies at 135 °C and 165 °C correspond to the transitions to the multi-cell cubic and single-cell cubic paraelectric phases, respectively, according to previous reports [11,17,18].

The ferroelectric phase in PNZST 43/8.0/2 can also be formed at 25 °C through an irreversible electric field-induced phase transition. Figure 4 shows polarization vs. electric field hysteresis loops for the very first two cycles on the antiferroelectric PNZST 43/8.0/2, with the first quarter cycle data highlighted in red. The antiferroelectric to ferroelectric transition occurs at 11.5 kV/cm (denoted as E_F in literature) during the first quarter cycle of loading. After the phase transition, the ceramic behaves like a normal ferroelectric composition, maintaining a large remnant polarization (P_R = 29.1 μC/cm^2) when the applied field is removed. The switching of the polarization occurs at the coercive field of 6.6 kV/cm (E_C). It should be noted that the electrical poling-induced ferroelectric phase in PNZST 43/8.0/2 has aligned polarizations while the cooling-induced ferroelectric phase presumably has random polarizations.

The stable ferroelectric state at 25 °C displays a crystal structure different from the antiferroelectric phase in the as-processed ceramic, as revealed by X-ray diffraction of the (200) peak shown in Fig. 5. The antiferroelectric phase in PNZST 43/8.0/2 is in a pseudo-tetragonal perovskite structure as evidenced by the peak splitting. In contrast, the peak splitting disappears in the ferroelectric phase induced by cooling or poling, suggesting a rhombohedral structure. The change in crystal symmetry is consistent with previous studies on similar compositions [33,36].

Figure 6 again compares the ferroelectric phases with the original antiferroelectric phase in PNZST 43/8.0/2 through Raman spectroscopy. A previous study [37] supports the finding from Fig. 6 that the ferroelectric phase results in a high intensity Raman peak at ~60 cm^{-1} and a low intensity peak at ~125 cm^{-1}, whereas the antiferroelectric phase shows a peak at ~80 cm^{-1}. The two phases are also easily distinguished through comparison of the slope between 70 cm^{-1} and 90 cm^{-1}, as indicated in Fig. 6. Due to its simplicity and independence on the signal-to-noise ratio of the spectra, the calculated slope is used to determine the ferroelectric phase during Raman mapping.

The transformation-toughening effect in antiferroelectric PNZST 43/8.0/2 is demonstrated with both indentation fracture experiments and R-curve measurements. Figure 7 shows representative optical microscopy images of Vickers indents on polished surfaces of as-processed, cooled, and poled PNZST 43/8.0/2 ceramic. The poling direction is indicated by the dark arrow in Fig. 7(c). Measurements on more than 10 indents for the as-processed and cooled specimens indicate average crack length ($2c$) values of 128 ± 5.3 μm in the as-processed ceramic and 167 ± 7.3 μm in the ceramic after dry ice cooling. Direct measurement of the indent shown in Fig. 7(c) indicates $2c$ values of ~131 μm in the poling field direction and ~188 μm perpendicular to the poling field direction in the electrically poled ceramic. The anisotropy in the crack length, hence the fracture toughness, in poled ferroelectric ceramics is consistent with previous studies [26,27]. Although indentation techniques may not provide accurate absolute fracture toughness values [34], the trend in the crack length implies that the ferroelectric phase, which has a larger specific volume, is formed at the indentation crack tip due to the presence of dilatational stresses and suggests that transformation toughening (a combined ferroelastic and phase-transition toughening) takes place in the as-processed antiferroelectric PNZST 43/8.0/2.

A more rigorous fracture mechanics experiment, R-curve measurements on compact tension specimens according to the ASTM E 1820-08 standard [38], was further implemented to demonstrate the phase transition toughening effect in antiferroelectric PNZST 43/8.0/2. The results are shown in Fig. 8, where the data from PNZST 43/6.4/2, a very similar antiferroelectric composition, are included as reference. Figure 8(a) indicates that the ferroelectric phase in PNZST 43/6.4/2 is not stable, and the ceramic returns to the antiferroelectric state when the applied field is removed. The data displayed in Fig. 8(b) clearly shows that PNZST 43/8.0/2 has a larger steady-state fracture toughness than PNZST 43/6.4/2.

The mode I crack growth resistance (K_{IR}) of the antiferroelectric ceramics shown in Fig. 8(b) can be characterized with three parameters: the steady state toughness K_∞, the toughening effect ΔK, and a fitting parameter λ [29,39].

$$K_{IR} = K_\infty + \Delta K \exp\left(-\lambda\sqrt{\Delta c}\right) \qquad (1)$$

K_∞ is determined to be 1.82 MPa√m for PNZST 43/8.0/2 and 1.18 MPa√m for PNZST 43/6.4/2, while ΔK is calculated to be -0.87 MPa√m for PNZST 43/8.0/2 and -0.43 MPa√m for PNZST 43/6.4/2. The fracture toughness for PNZST 43/8.0/2 is hence 54% higher than PNZST 43/6.4/2. The results confirm that an irreversible phase transition is necessary for the toughening effect to function [3]. Compared to the fracture toughness values from our recent R-curve measurement on compact tension specimens of ferroelectric $Pb(Zr,Ti)O_3$ ceramics [29], the K_∞ in antiferroelectric PNZST 43/8.0/2 is 60 to 127% higher. It should be noted that the initial toughness values at $\Delta c = 0$ are prone to greater variability than the steady state toughness values.

In order for the phase-transition-toughening effect to work, the induced phase must have a larger specific volume that can be triggered by proper dilatational stresses and remains when the stimuli are removed [3,4]. Results in Figs. 3 through 6 indicate that the ferroelectric phase in

PNZST 43/8.0/2 has a larger volume, which can be triggered by cooling or electrical poling, and is stable at room temperature (25 °C). Data from fracture measurements in Figs. 7 and 8 indirectly suggest that the ferroelectric phase can also be triggered by dilatational stresses and lead to a strong toughening effect. To directly confirm the formation and retention of the ferroelectric phase, Raman mapping was performed around the tip of a Knoop indentation crack on the polished surface of an as-processed antiferroelectric PNZST 43/8.0/2 ceramic. Figure 9(a) shows an optical micrograph of the indentation crack, where the crack tip is marked with a white cross. As explained in the last section, the slope of the Raman spectra between 70 cm^{-1} and 90 cm^{-1} was used to determine the ferroelectric phase fraction during the mapping. The map of this crack after indentation is shown in Fig. 9(b), where the dark red color represents the ferroelectric (FE) phase and the dark blue color indicates the antiferroelectric (AFE) phase. The crack tip on this map is indicated by the cross at the (0,0) position. The irregular shape of the phase transition zone is believed to originate primarily from the random crystallographic orientation of the grains. It is also noted that the transition zone revealed in Fig. 9(b) is very small when compared to ferroelastic toughening of $Pb(Zr,Ti)O_3$ [24,25] or phase transition toughening of ZrO_2-based ceramics [4]. The main reason is that the indentation crack is only ~10 μm (Fig. 9a), far from reaching the steady state. Nonetheless, the Raman mapping results provide direct evidence that the ferroelectric phase was formed during indentation and remains in the vicinity of the crack tip across tens of microns after the indentation load is removed.

Presumably the phase transition zone should expand under tensile stresses. This is supported by Raman mapping of the crack under a 7.5 kV/cm *in-situ* applied DC field, shown in Fig. 9(c). It is noted that this nominal field is still below the critical field E_F (11.5kV/cm). However, the presence of the crack intensifies the actual field around the crack tip [40]. As a

result, the ferroelectric phase is induced electrically. Since similar stress intensification is expected from a crack as well, applying a sub-critical nominal tensile stress is expected to expand the phase transition zone in a similar manner. The Raman mapping, therefore, verifies the stress induced phase transition and the resulting toughening effect.

4. Discussion

To explain the observed phenomena, we imagine that the stress-induced antiferroelectric to ferroelectric transformation takes place in two processes: the transition of the as-processed antiferroelectric phase to a ferroelectric phase with random orientations and then ferroelastic switching of the ferroelectric phase to an aligned state [41]. The former involves only dilatational deformation with volumetric strain, θ_t, while the latter involves a pure deviatoric deformation with shear strain, γ_s. The decoupling of the two processes defines four different states of the material: the random antiferroelectric (AFEr) state, the random ferroelectric (FEr) state, the aligned antiferroelectric (AFEa) state, and the aligned ferroelectric (FEa) state, as shown in Fig. 10(a). It should be noted that not all of the four states are necessarily stable, and the actual physical process may well involve simultaneous phase transition and domain switching. The final state is independent of the transformation pathway, and the two imaginarily decoupled steps are introduced only to simplify the following estimation of toughening.

Correspondingly, the process zone near a crack tip consists of at least two regions, as depicted in Fig. 10(b) and (c). For a stationary crack, the antiferroelectric-to-ferroelectric transition zone, shown by the solid curve on the figures, has a wider shape encompassing the region in front of the crack tip where the local stress state is the most triaxial. The ferroelastic domain-switching zone, shown by the dash curve, appears at an angle from the crack face, where

the shear stress is maximized [42]. Only in the overlapping region, the material is transformed and switched into an FEa state. For simplicity, the partially transformed/switched zones are omitted from the diagrams in Fig. 10(b) and (c).

For a propagating crack, the irreversible processes in the process zone leave a wake behind the advancing crack tip. From the classic transformation-toughening theory, the existence of the wake is essential to the toughening mechanism [3,43,44]. In the absence of an applied electric field, the ferroelastic domain switching is primarily irreversible, i.e. the aligned state will not switch back to a random state upon mechanical unloading [6]. Therefore, the switching zone always leaves behind a wake, as sketched in Fig. 10(b) and (c). The reversibility of the antiferroelectric-ferroelectric phase transition, on the other hand, is dependent on the composition and temperature [17,33]. For a material with reversible transition, the grains in the transformed zone would recover to the antiferroelectric phase but remain switched, as shown by Fig. 10(b). For such a material like PNZST 43/6.4/2, ferroelastic domain switching is the only toughening mechanism. For a material with irreversible transition, the wake may consist of two bands, originated from the two regions in the crack tip process zone. Both mechanisms contribute to the toughening of the material such as PNZST 43/8.0/2. (It is unknown whether the switching zone is larger than the transition zone. Fig. 10(c) illustrates the case when the switching zone is larger. In the case when the transition zone is larger, the wake will consist of a FEa band inside an AFEa band.)

Many models of transformation toughening exist in literature, but most either address a volumetric transformation or a deviatoric domain switching [3,43,45]. A few models account for a general transformation with both volumetric and deviatoric components [44]. Here, for the purpose of illustration and qualitative estimation, we make the assumptions that the two

mechanisms, both driven by the remote stress intensity factor K_∞, are independently generated, and that their contributions can be superimposed to give the overall toughening effect, $\Delta K = \Delta K_t + \Delta K_s$ (ΔK_t denotes the phase-transition contribution while ΔK_s marks the ferroelastic-switching contribution). While the latter can be justified through the small scale transformation assumption and the linear superposition of elasticity, the former is introduced mainly for simplicity, as the study of the interaction between the two process zones is beyond the scope of the present article. Here, we also neglect the difference between the ferroelastic switching in antiferroelectric and ferroelectric phases and do not distinguish between the transformation strains γ_s and γ_s' or the corresponding critical stresses.

Following Budiansky et al. [43], we estimate the steady-state toughening due to dilatational phase transition

$$\frac{\Delta K_t}{K_\infty} \approx -0.046 \frac{Y(1+\nu)\theta_t}{(1-\nu)X_c} \qquad (2)$$

where Y is Young's modulus, ν is Poisson's ratio, and X_c is the critical hydrostatic stress for the transition. The toughening due to deviatoric domain switching can be estimated as [46,47]:

$$\frac{\Delta K_s}{K_\infty} \approx -0.031 \frac{Y\gamma_s}{(1-\nu^2)\tau_c} \qquad (3)$$

Let us first consider the composition PNZST 43/8.0/2, which has an irreversible transition. Using the strain data measured on PNZST 43/7.5/2 [17], the volumetric transition strain $\theta_t = 0.38\%$ and a switching shear strain $\gamma_s = 0.14\%$. The critical stresses for transition and switching are taken from measurements on materials of similar compositions, $X_c = 110\text{MPa}$ [19] and $\tau_c = 25\text{MPa}$ [22], respectively. Further taking the representative values of the modulus and Poisson's ratio,

$Y = 100\text{GPa}$ and $\nu = 0.3$, we can estimate the toughening contributions from the two mechanisms

$$\frac{\Delta K_t}{K_\infty} \approx -0.3 \qquad (4)$$

and

$$\frac{\Delta K_s}{K_\infty} \approx -0.2 \qquad (5)$$

The total toughening effect $\frac{\Delta K}{K_\infty} \approx -0.5$ agrees very well with the experimental value. Now let us consider the composition PNZST 43/6.4/2 with a reversible phase transition. Considering the polycrystalline nature of the material, we take the effective switching strain to be half of the single crystal value, $\gamma_s = 0.3\%$, and use the same critical stress, $\tau_c = 25\text{MPa}$. The ferroelastic switching toughening is estimated as

$$\frac{\Delta K_s}{K_\infty} \approx -0.4 \qquad (6)$$

Again, the estimation agrees well with the measured value.

5. Conclusions

Antiferroelectric ceramics of solid solutions $Pb_{0.99}Nb_{0.02}[(Zr_{0.57}Sn_{0.43})_{1-y}Ti_y]_{0.98}O_3$ with compositions y = 0.07 ~ 0.08 display an irreversible transition to the ferroelectric phase with a volume expansion at room temperature. Through indentation fracture and compact tension crack growth study, a phase-transition-toughening effect is demonstrated to occur in the model composition PNZST 43/8.0/2. This ceramic displays a fracture toughness of 1.82 MPa√m and a toughening effect of -0.87 MPa√m at 25 °C. The fracture toughness measured in this ceramic is ~50% higher than other compositions with a reversible antiferroelectric-ferroelectric phase

transition, and 60% ~ 130% higher than ferroelectric $Pb(Zr,Ti)O_3$ ceramics. It is suggested that both phase transition and ferroelastic switching contribute to the enhanced toughness. Through further fine tune of the chemical composition and careful manipulation of the phase transition, an even higher fracture toughness can be realized in this solid solution system.

Acknowledgements

This work was supported by the National Science Foundation (NSF) through Grant CMMI-1027873.

References

[1] Frieman SW, White GS. J Intell Mater Systems and Struct 1995;6:49.

[2] Garvie RC, Hannink RH, Pascoe RT. Nature 1975;258:703.

[3] McMeeking RM, Evans AG. J Am Ceram Soc 1982;65:242.

[4] Hannink RHJ, Kelly PM, Muddle BC. J Am Ceram Soc 2000;83:461.

[5] Calvie E, Joly-Pottuz L, Esnouf C., Douillard T, Gremillard L, Malchere A, Chevalier J, Masenelli-Varlot K. Acta mater 2013;61:174.

[6] Mehta K, Virkar AV. J Am Ceram Soc 1990;73:567.

[7] Chantikul P, Bennison SJ, Lawn BR. J. Am. Ceram. Soc. 1990;73:2419.

[8] Dougherty JP. U.S. Patent 5,545,184, 1996.

[9] He H, Tan X. Appl. Phys. Lett. 2004;85:3187.

[10] Kwon S, Hackenberger W, Alberta E, Furman E, Lanagan M. IEEE Electr Insul M 2011;27: 43.

[11] Young SE, Zhang JY, Hong W, Tan X. J Appl Phys 2013;113:054101.

[12] Berlincourt D, Krueger HHA, Jaffe B. J Phys Chem Solids 1964;25:659.

[13] Tan X, Jo W, Granzow T, Frederick J, Aulbach E, Rödel J. Appl Phys Lett 2009;94:042909.

[14] Pan WY, Dam CQ, Zhang QM, Cross LE. J Appl Phys 1989;66:6014.

[15] Tan X, Frederick J, Ma C, Aulbach E, Marsilius M, Hong W, Granzow T, Jo W, Rödel J. Phys Rev B 2010;81:014103.

[16] Brodeur RP, Gachigi KW, Pruna PM, Shrout TR. J Am Ceram Soc 1994;77:3042.

[17] Frederick J, Tan X, Jo W. J Am Ceram Soc 2011;94:1149.

[18] Viehland D, Forst D, Xu Z, Li JF. J Am Ceram Soc 1995;78:2101.

[19] Dai Z, Xu Z, Yao X. Appl Phys Lett 2008;92:072904.

[20] Zhou LJ, Zimmermann A, Zeng YP, Aldinger F. J Am Ceram Soc 2004;87:1591.

[21] He H, Tan X. J Am Ceram Soc 2007;90:2090.

[22] Tan X, Ma C, Frederick J, Beckman S, Webber KG. J Am Ceram Soc 2011;94:4091.

[23] Sluka T, Webber K, Colla E, Damjanovic D. Acta mater 2012;60:5172.

[24] Kounga Njiwa AB, Lupascu DC, Rödel J. Acta mater 2004;52:4919.

[25] Jones JL, Motahari SM, Varlioglu M, Lienert U, Bernier JV, Hoffman M, Ustundag E. Acta mater 2007;55:5538.

[26] Schneider GA, Heyer V. J Euro Ceram Soc 1999;19:1299.

[27] Fu R, Zhang TY, J Am Ceram Soc 2000;83:1215.

[28] Karastamatis T, Lupascu DC, Lucato SLS, Rödel J, Lynch CS. J Euro Ceram Soc 2003;23:1401.

[29] Seo YH, Bencan A, Koruza J, Malic B, Kosec M, Webber KG. J Am Ceram Soc 2011;94:4419.

[30] Xu Z, Viehland D, Payne DA. J Mater Res 1995;10:453.

[31] He H, Tan X. Phys Rev B 2005;72:024102.

[32] Cao HC, Evans AG. J Am Ceram Soc 1993;76:890.

[33] Tan X, Frederick J, Ma C, Jo W, Rödel J. Phys Rev Lett 2010;105:255702.

[34] Evans AG, Marshall DB. J Am Ceram Soc 1981;64:C182.

[35] Deluca M, Bermejo R, Grunbichler H, Presser V, Danzer R, Nickel KG. Scripta mater 2010;63:343.

[36] Blue CT, Hicks JC, Park SE, Yoshikawa S, Cross LE. Appl Phys Lett 1996;68:2942.

[37] He H, Tan X. J Phys Condens Matter 2007;19:136003.

[38] ASTM Standard E 1820-08, ASTM International, West Conshohocken, PA, 2008.

[39] Fett T, Munz D. Arch Appl Mech 2006;76:667.

[40] McMeeking RM. J Appl Math Phys (ZAMP) 1989;40:615.

[41] Park SE, Pan MJ, Markowski K, Yoshikawa S, Cross LE. J Appl Phys 1997;82:1798.

[42] Shang JK, Tan X. Acta mater 2001;49:2993.

[43] Budiansky B, Hutchinson JW, Lambropoulos JC. Int J Solids Struct 1983;19:337.

[44] Lambropoulos JC. Int J Solids Struct 1986;22:1083.

[45] Yang W, Zhu T. J Mech Phys Solids 1998;46:291.

[46] Reece MJ, Guiu F. J Euro Ceram Soc 2001;21:1433.

[47] Landis C. J Mech Phys Solids 2003;51:1347.

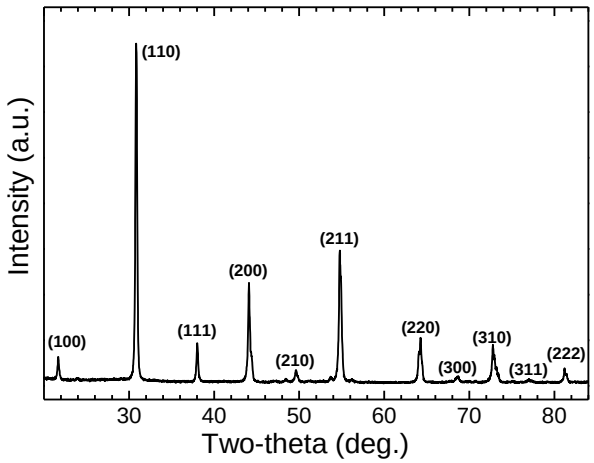

Fig. 1. X-ray diffraction spectrum of the antiferroelectric PNZST 43/8.0/2 ceramic prepared with hot isostatic press. The peaks are indexed according to a pseudocubic perovskite structure.

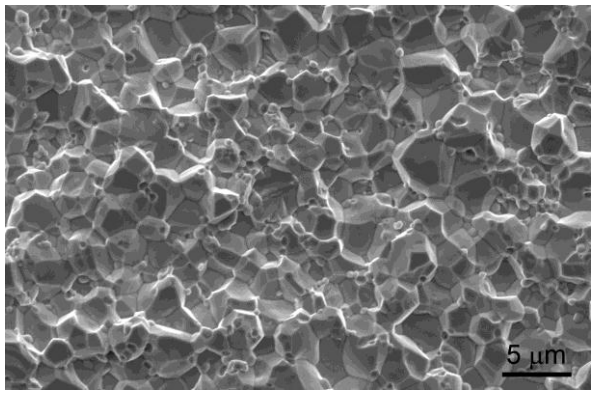

Fig. 2. Scanning electron microscopy micrograph of the PNZST 43/8.0/2 ceramic.

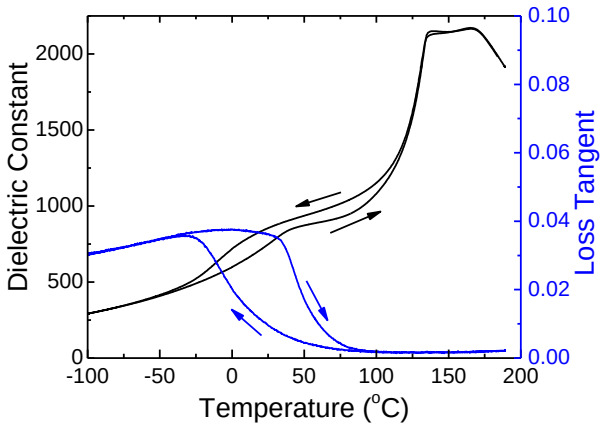

Fig. 3. Dielectric measurements at 1 kHz and 3 ^{o}C/min. during heating and cooling of the PNZST 43/8.0/2 ceramic. Error bars are of the order of the line thickness and are not shown.

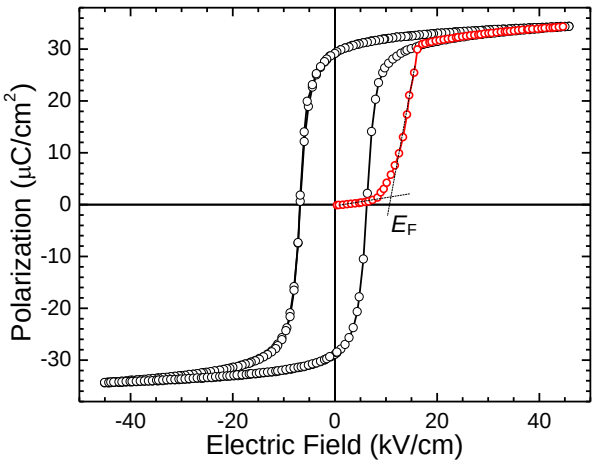

Fig. 4. The first two cycles of the polarization vs. electric field hysteresis loop of the PNZST 43/8.0/2 ceramic measured at 25 ^{o}C and 4 Hz.

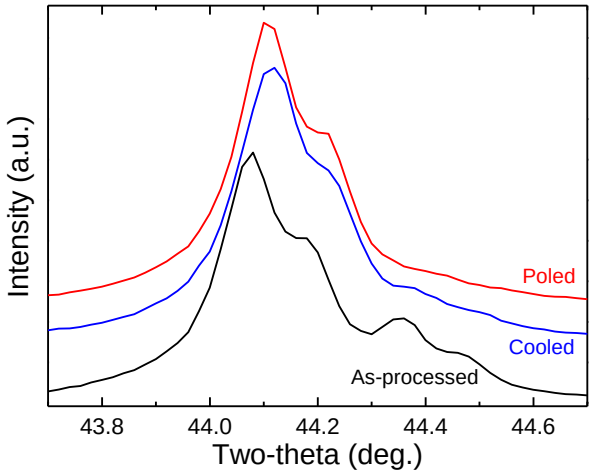

Fig. 5. Close examination of the pseudocubic (200) peak of the as-processed, cooled, and poled PNZST 43/8.0/2 ceramic.

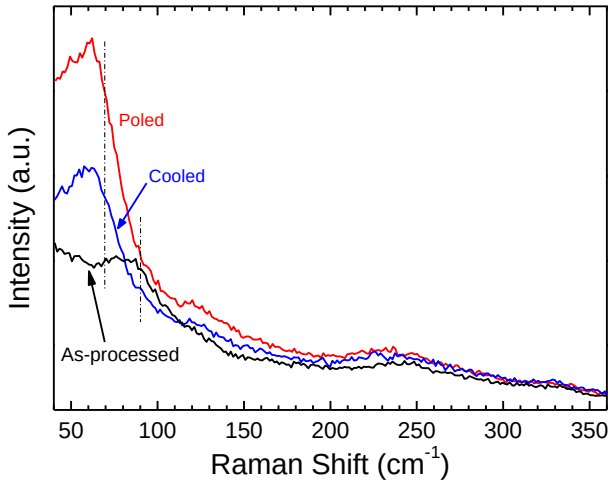

Fig. 6. Raman spectra of the as-processed, cooled, and poled PNZST 43/8.0/2 ceramic.

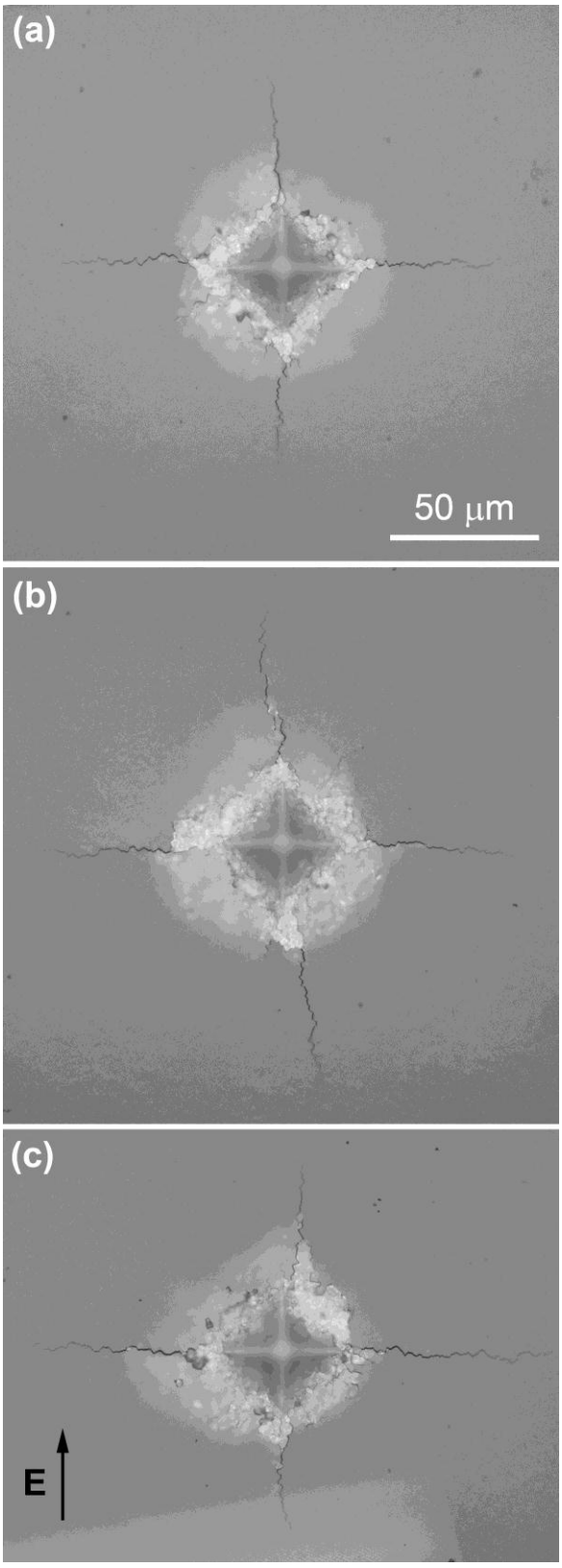

Fig. 7. Vickers indents of the (a) as-processed, (b) cooled, and (c) poled PNZST 43/8.0/2 ceramic.

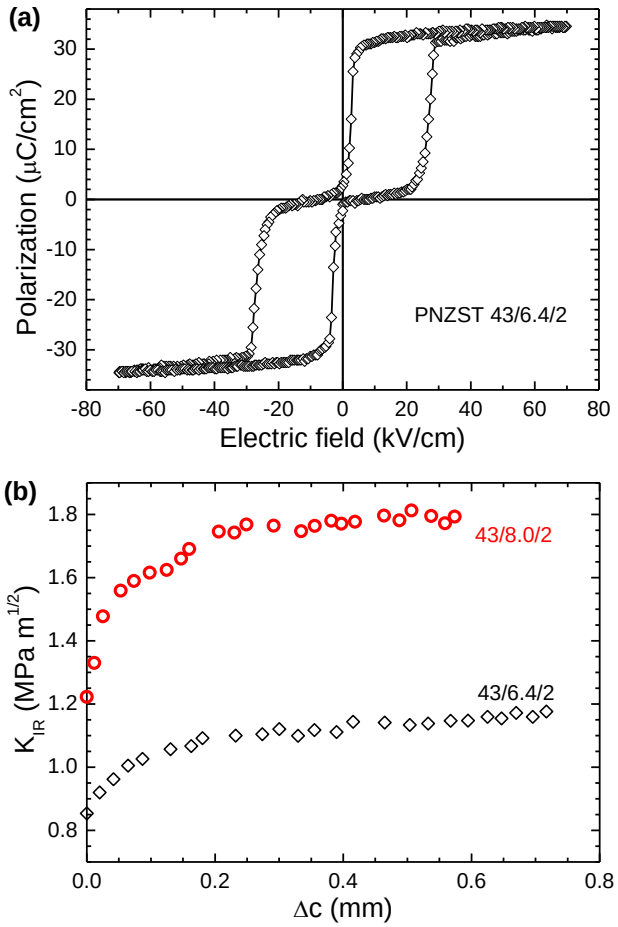

Fig. 8. (a) The polarization vs. electric field hysteresis loop of the PNZST 43/6.4/2 ceramic measured at 4 Hz and 25 ^{o}C. (b) Fracture resistance curves measured from compact-tension specimens at 25 ^{o}C. Error bars are less than the symbol size and are not shown.

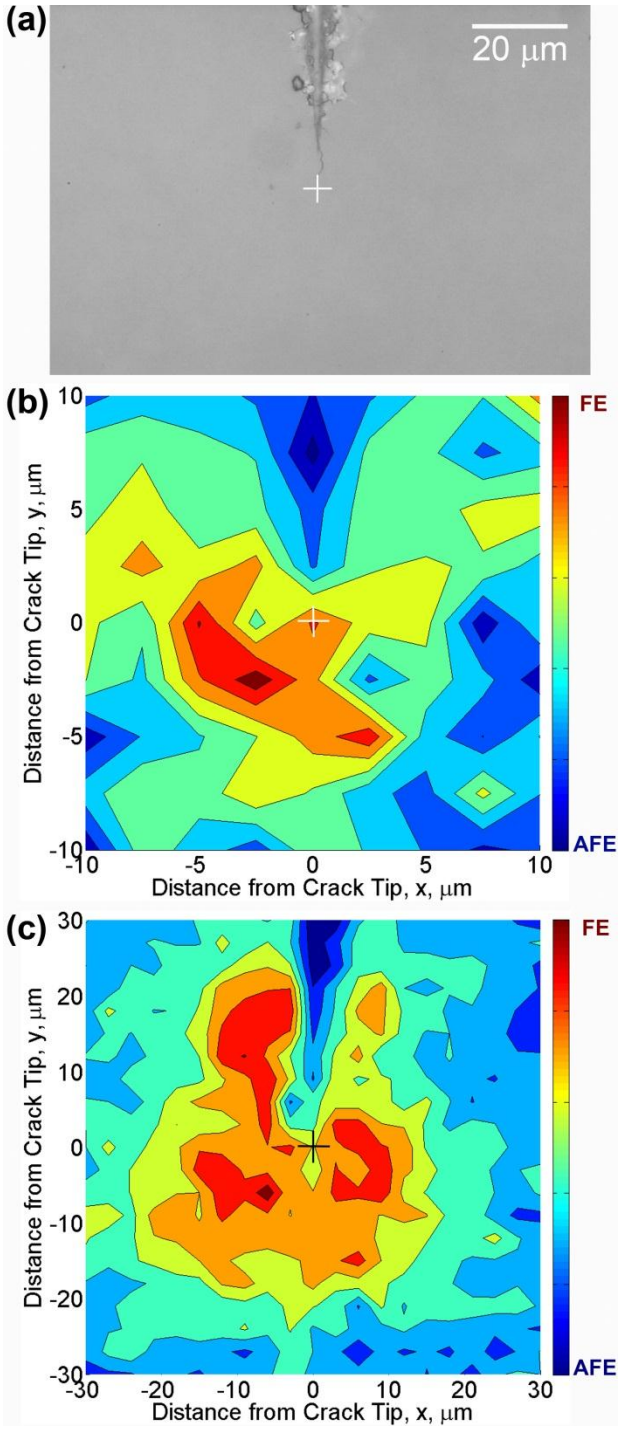

Fig. 9. Raman mapping of the antiferroelectric and ferroelectric phases in the vicinity of a Knoop indentation in the PNZST 43/8.0/2 ceramic. The crosses mark the crack tip. (a) The Knoop indentation, (b) the induced ferroelectric phase after the indentation, (c) the induced ferroelectric phase under an applied field of 7.5 kV/cm along the *x* direction.

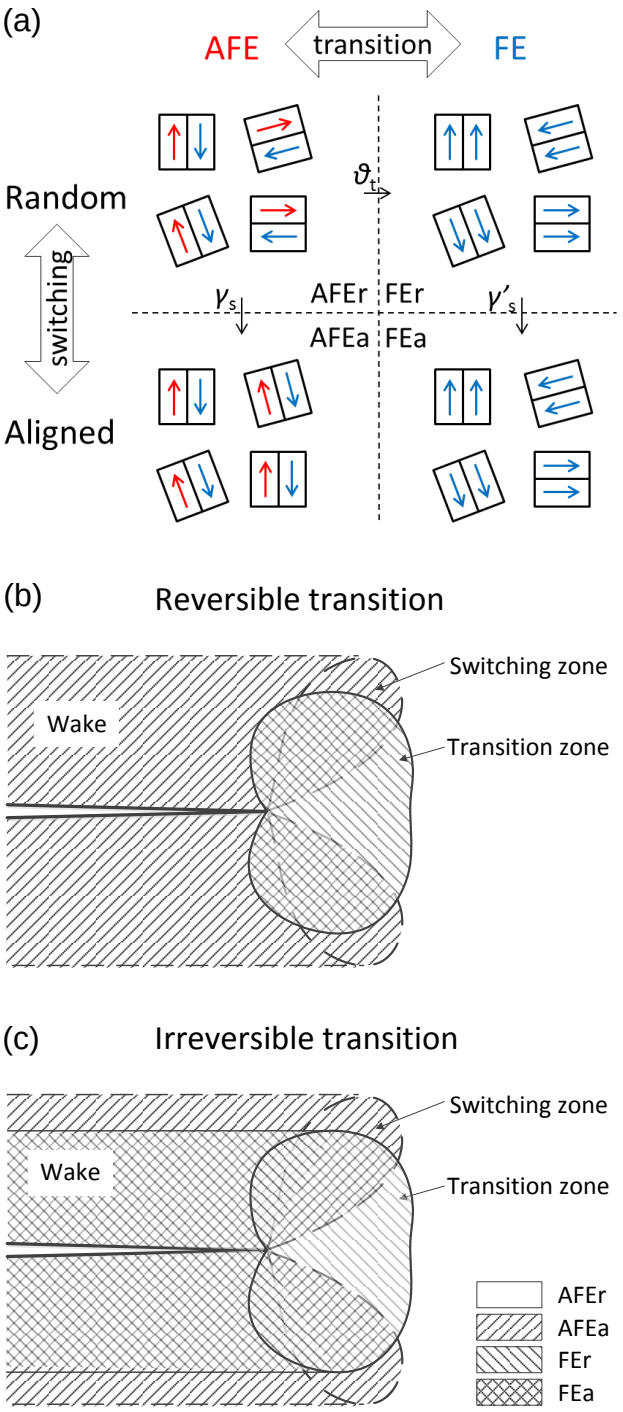

Fig. 10. Simplified schematic diagrams to explain the transformation toughening mechanisms. (a) The four possible states for the material in the process zone, (b) the likely scenario for a reversible antiferroelectric-ferroelectric phase transition, (c) the likely scenario when the transition is irreversible.